Nanometer scale chemomechanical characterization of antiwear films

M.A. Nicholls[a], P.R. Norton[a,*], G.M. Bancroft[a], M. Kasrai[a],
T. Do[b], B.H. Frazer[c] and G. De Stasio[c]

[a]University of Western Ontario, London, Ontario, Canada N6A 5B7
[b]Atomic Energy of Canada Ltd., Chalk River, Ontario, Canada
[c]University of Wisconsin-Madison, USA

We report the first nanometer scale chemical and mechanical (chemomechanical) characterization of selected features of a tribologically derived zinc dialkyl-dithiophosphate (ZDDP) antiwear film. AFM permits identification of the features responsible for preventing wear. These features are identified by nearby microscale fiducial marks, and their mechanical properties are determined by imaging nanoindentation. The same features are then studied by X-ray photoelectron emission microscopy (X-PEEM), which provides both elemental and chemical information at ∼200 nm spatial resolution. The mechanical properties are then determined for the same features, which are formed of a polyphosphate glass. This information provides new insights into the mechanisms by which ZDDP antiwears films are effective at inhibiting asperity contact between two metal surfaces.

KEY WORDS: ZDDP, XANES, nanoindentation, tribology, mechanical properties, X-ray spectromicroscopy, antiwear film

1. Introduction

Zinc dialkyl-dithiophosphates (ZDDPs) are primary antiwear and antioxidant additives in all commercial motor oils. It has been clearly established that ZDDPs break down under rubbing conditions to create thin antiwear films [1–5]. Film formation and kinetics are important in preventing wear, since the film is responsible for limiting the contact between the two rubbing surfaces. ZDDPs, their reaction products, and antiwear films have been studied by many analytical techniques such as Auger electron spectroscopy (AES) [6,7], energy dispersive X-ray (EDX) mapping [8,9], X-ray photoelectron spectroscopy (XPS) [10,11], time-of-flight secondary mass spectrometry (ToFSIMS) [12], X-ray absorption spectroscopy (XAS) [1–3,13–15], and the film has been found to contain varying amount of zinc, phosphorous, oxygen, sulfur, and iron. X-ray absorption near edge spectroscopy (XANES) analysis [1–3,13–15] has shown that the film is formed of polyphosphate glasses that presumably contain mostly zinc as the countercations. The two modes of XANES analysis, using fluorescence and total electron yield detection provide different depth sensitivities. This has been used to deduce that the film is actually a layered system and the surface of the film is composed primarily of long-chain polyphosphates and the bulk primarily

of shorter-chain polyphosphates [13]. Understanding the mechanisms of film formation is beneficial to understanding how it prevents asperities from coming into contact.

ZDDP antiwear films have also been micro-characterized using imaging techniques such as scanning electron microscopy (SEM) [16–18], atomic force microscopy (AFM) [19,20] and imaging nanoindenters [19–23]. These techniques are all in agreement that the ZDDP antiwear film is laterally and vertically heterogeneous, being composed of ridges and valley regions. The ridge regions are composed of raised patches of film that have been termed antiwear pads [19,20]. It has been suggested that these pads are responsible for bearing the load between the two rubbing surfaces and limiting the contact between the asperities, thereby reducing wear [20]. The antiwear films and pads have been studied using nanoindentation, and found to have unique mechanical properties. The ridge regions have a stiffer response than the lower valley regions, exhibiting indentation moduli (E_s^*) of ∼85 and ∼30 GPa respectively [19–21,23,24]. The difference in moduli was attributed to the extent to which the ZDDP has been transformed to polyphosphate glass, and this is representative of the film history. Thus the valley regions contain partially decomposed ZDDP, wear debris, and partially formed antiwear film, while the ridge regions are antiwear pads composed of polyphosphate glass formed from fully decomposed ZDDP. The mechanical properties of the large

*To whom correspondence should be addressed. E-mail: mnicholl@ uwo.ca

antiwear pads have been found be laterally heterogeneous, with the center of the pads being stiffer than the edges, suggesting that the higher loads experienced at the center of the film may be responsible for creating pressures and temperatures that can cause cross-linking between the polyphosphate chains and generating a stiffer material [20].

To-date, there are very few additives that have such an important impact on prolonging the life of an engine; but despite years of work, the mechanisms of formation and action of the antiwear films are poorly understood. Phosphorus- and zinc-free additives are urgently needed due to tighter environmental laws being applied; this will ultimately lead to the elimination of ZDDP in motor oils. We believe that a rational approach to the synthesis of new ashless and phosphate-free additives requires an understanding of why ZDDPs work as effectively as they do. Advances in X-ray spectromicroscopy can now provide spatially resolved XANES analysis at the < 100 nm nanometer length scale [25–28]. A comparison of the spatially resolved microchemistry, morphology and nanomechanical properties of selected features in a ZDDP antiwear film, through the use of X-PEEM and scanning probe techniques, will provide a detailed understanding into the nature and growth of the film. This is the first time that such a nanoscale correlation between the observed elastic response of selected features in the antiwear film and their chemistry has been attempted.

2. Experimental

2.1. Glass synthesis procedure

The starting materials for the synthesis of zinc polyphosphates is zinc metaphosphate ($Zn(PO_3)_2$) and ZnO (99.99%, Alfa). The metaphosphate was prepared by mixing equal molar proportions of ZnO and P_2O_5 (99.99%, Aldrich). The glasses were prepared using the method described in literature [29]. All preparations were carried out in silica glass tubes. A slight excess of P_2O_5 was added to compensate for any loss during heating. The zinc metaphosphate was characterized by powder X-ray diffraction (XRD) and was a crystalline phase consistent with the PDS reference material. The zinc polyphosphate glasses were characterized by powder XRD and electron probe microanalysis (EPMA). From the atomic proportions determined by EPMA the error in chain length for the $Zn_4P_6O_{19}$ glass is ±1 PO_4 unit, $Zn_6P_{10}O_{31}$ is ±2 PO_4 units, $Zn_{10}P_{18}O_{55}$ is ±4 PO_4 units, $Zn_{20}P_{38}O_{115}$ ±3 PO_4 units. Small amounts of the polyphosphate glasses were gently pressed onto carbon tape and inserted into vacuum for X-ray absorption near edge structure (XANES) analysis.

2.2. ZDDP antiwear film formation

The ZDDP antiwear films were formed in a reciprocating Plint wear tester under boundary lubrication conditions with a cylinder-on-flat test geometry establishing a line contact. The test conditions consisted of a rubbing time of 1 h, at 100 °C, with an applied load of 220N, and a frequency of 25 Hz under a fully flooded state. The Hertzian contact pressure, for a line contact between these materials, is 0.504 GPa. The ZDDP solution was a commercial ZDDP obtained in pre-concentrated form from Imperial Oil, Canada. The commercial concentrate is a mixture of neutral and basic forms, consisting of secondary butyl (85%) and *n*-octyl (15%) groups. The concentrate was diluted using MCT-10 base oil to 1.2 mass% resulting in a phosphorus content of ∼0.1% by weight. MCT-10 base oil is a mineral oil with a maximum sulfur content of 0.25 mass%. The steel samples were manufactured from AISI 52100 steel into square specimens 10 mm × 10 mm × 4 mm in thickness. The reciprocating cylinder was also manufactured from AISI 52100 steel with 6 mm diameter and 6 mm length. The steel samples and pins were austenitized and quenched, their hardness was > 60 Rockwell C. The pins were used as is, and the steel coupons were polished using 3 μm diamond paste giving a average surface roughness of ∼7 nm determined by AFM image analysis. The films were removed from the oil bath and gently wiped with tissue paper. The samples were then washed with hexanes by rinsing the sample for ∼15 s from a spray-bottle, at room temperature, before analysis. A grid composed of fiducial marks was created using a Vickers hardness tester using loads of 100 and 500 g which made indents ∼25 and ∼150 μm across respectively. This grid allowed for relocation of the same regions with the multiple techniques discussed below.

2.3. XANES and X-PEEM analysis

XANES spectroscopy was performed at the 1 GeV Aladdin storage ring, University of Wisconsin, Madison. XANES analysis employs the use of soft X-rays making it a non-destructive technique. The phosphorous L-edge data were obtained using the Grasshopper beamline in which the X-ray beam is monchromated by an 1800 g/mm grating and has a resolution of ∼0.2 eV at the P L-edge. Spectra were recorded using the total electron yield (TEY) and fluorescence yield (FY) detection modes. The sampling depths of the TEY and FY at the P L-edge are ∼5 and ∼60 nm respectively [30]. At least two individual scans were recorded for each specimen and digitally combined. The spectra were normalized against I_0 and a linear background was subtracted. Due to the method used for the preparation of the polyphosphate glasses, some unreacted P_2O_5 on the surface of the polyphosphate crystals distorted the spectra so the FY spectra of the

zinc polyphosphate glasses are shown here, because they are more representative of the bulk composition. X-PEEM was performed using the SPHINX (Frazer *et al.* submitted for publication) microscope (ELMI-TEC GmbH) installed on the 6m-TGM (toroidal grating monochromator) beamline at the 1 GeV Aladdin storage ring, University of Wisconsin, Madison. The high-energy grating was optimized to give ~0.1 eV resolution at the P L-edge. P L-edge images were taken with a step size of 0.1 eV, and 100 μm field of view for the energy region 130–160 eV. Image intensity in X-PEEM is proportional to the TEY and the surface sensitivity was limited by the escape depth of the secondary electrons at the P L-edge (3–5 nm) [30,31]. The SPHINX uses a combination of seven stigmators and deflectors and six magnetic lenses to focus and magnify the secondary electron image. This image is projected onto a multichannel plate and phosphor screen assembly where it is recorded by a 12 bit digital camera. The resolution obtained in these images was chosen to be ~200 nm per pixel. The 301 images (0.1 eV step size) were combined to produce a three-dimensional data set or spectromicroscopy 'stack' [27] that was analyzed to extract detailed phosphorous information about the tribofilm. Images were dominated by topography, charging, work function effects, and shadowing, all due to the inherent heterogeneous nature of a ZDDP tribofilm and how it is prepared. Nevertheless detailed, spatially resolved chemical information could still be obtained from the data.

2.4. Nanomechanical property testing

A NanoScope IIIa atomic force microscope from Digital Instruments® was used to identify topographic regions of interest and to investigate the morphology of the antiwear films. Mechanical properties of the films were measured with a hybrid system composed of a Triboscope force transducer from Hysitron Inc® and an AFM-1 base from Digital Instruments®. This tandem system allows for constant force imaging of the sample surface using the PZT scanner of the AFM to control the x–y positioning of the sample, and the transducer monitors the motion of the tip and measures the indentation force. This tandem system allows a user to image the surface of a sample, with a resolution of ~100 nm or better, and quantitatively measure the nanomechanical properties of selected features on the antiwear film. The indenter tip is a three-sided Berkovich diamond. The average tip radius of a Berkovich diamond is between 100 and 160 nm. Accurate measurement of the displacement of the tip during the indentation process allows for the calculation of the hardness and reduced elastic modulus (E^*) of a feature from a force–displacement (*f–d*) curve. The values were calculated from the initial slope of the withdrawal

curve as suggested by Oliver and Pharr [32]. The system was calibrated for compliance and tip abnormalities, using the commonly accepted method of measuring a succession of indents into fused silica at different penetration depths to calculate the tip area function [33,34]. The reduced elastic modulus is defined through equation (1),

$$\frac{1}{E^*} = \frac{(1 - v_s^2)}{E_s} + \frac{(1 - v_i^2)}{E_i}, \tag{1}$$

where E_s and v_s are the Young's modulus and Poisson's ratio of the sample respectively, and E_i and v_i are the respective values for the indenter. The values listed in this report are the indentation modulus of the sample E_s^*, given by

$$E_s^* = \frac{E_s}{(1 - v_s^2)} = \left[\frac{1}{E^*} - \frac{(1 - v_i^2)}{E_i} \right]^{-1} \tag{2}$$

in which the tip properties have been removed from the reduced modulus value ($E_i = 1140$ GPa; $v_i = 0.07$) in equation (1). Indents were taken along antiwear pads and ridges that were within the region analyzed by X-PEEM imaging, and in areas chosen for their relevance to the understanding of the formation and method of wear reduction by ZDDP antiwear films. The indents were spaced > 300 nm apart to avoid the influence of the plastically deformed regions from the previous indents. Care was taken to use a maximum load that kept the penetration depth low, and hence minimize the possibility of forming pile-up and exceeding the 10% rule-of-thumb for measuring mechanical properties of soft films on a rigid substrate [33,35–37]. Topographic images were taken before and after each indent using the same tip that was used for the nonoindentation procedure.

There are several alternative approaches to the calculation of elastic moduli for thin films on rigid substrates [36–43]. In many cases these approaches are suggested for penetration depths greater than 10% of the thickness of the film. In an attempt to fully understand the mechanical response of the ZDDP films, and without fully knowing the *absolute* steel morphology below our film, the Song and Pharr method [42] of determining the elastic modulus is included. For a perfect Berkovich tip, the radius of contact, a, at a particular indentation depth can be estimated from the contact area of the indenter $A = 24.5h_c^2$, where h_c is the contact depth defined by,

$$h_c = h_{max} - 0.75 \frac{P_{max}}{S}, \tag{3}$$

where h_{max} and P_{max} are the maximum depth of penetration and load respectively and S is the slope of the

initial portion of the unloading curve and the relationships [41]:

$$A = \frac{\delta^2}{\alpha} \qquad (4)$$

$$\alpha = \frac{\delta}{2\beta} \qquad (5)$$

in which α and β are 0.03705 and 0.1731 for a perfect Berkovich tip [41]. The indentation modulus of the film can be separated from that of the steel using the Song and Pharr method [42], equations (6) and (7) are:

$$\frac{1}{E_s^*} = (1 - I_0)\frac{1}{E_{steel}} + I_0\frac{1}{E_f}, \qquad (6)$$

where

$$\begin{aligned} I_0 = & \frac{2}{\pi}\arctan\left(\frac{t}{a}\right) + \frac{1}{2\pi(1-v)} \\ & \times \left[(1-2v)\frac{t}{a}\ln\frac{1+(t/a)^2}{(t/a)^2} - \frac{(t/a)}{1+(t/a)^2}\right] \end{aligned} \qquad (7)$$

and E_s^* is the indentation modulus of the sample (film + steel; defined above), E_f is the modulus of the film, $E_{steel} = 220$ GPa, t *is* the film thickness, and assuming the Poisson's ratio for steel and the film are the same $v_{steel} = v_f = v = 0.3$.

3. Results and discussion

3.1. Zinc polyphosphate glasses

As described above, a series of amorphous zinc polyphosphate glasses with different chain lengths were synthesized and analyzed using XANES analysis. The glasses were determined to be amorphous by XRD analysis. These were used to calibrate the P L-edge XANES spectra as a function of chain length. This information was used to analyze the X-PEEM spectra at the P L-edge to determine the polyphosphate chain length. Previous work by others [44–46] has shown, using ³¹P NMR, Raman Spectroscopy and high performance liquid chromatography, that as the ratio of P_2O_5/ZnO increases so also does the length of the polyphosphate chains. Figure 1 shows the XANES spectra of two-dimensional polyphosphate glasses [47] (the terminology "two-dimensional" is used to denote the absence of cross-linking that would lead to three-dimensional chains). Also included is the spectrum of a three-dimensional zinc metaphosphate glass (of formula $Zn(PO_3)_2$) which has the largest degree of cross-linking [48].

The L-edge spectra are characterized by fine structure due to the spin–orbit splitting of the phosphorus
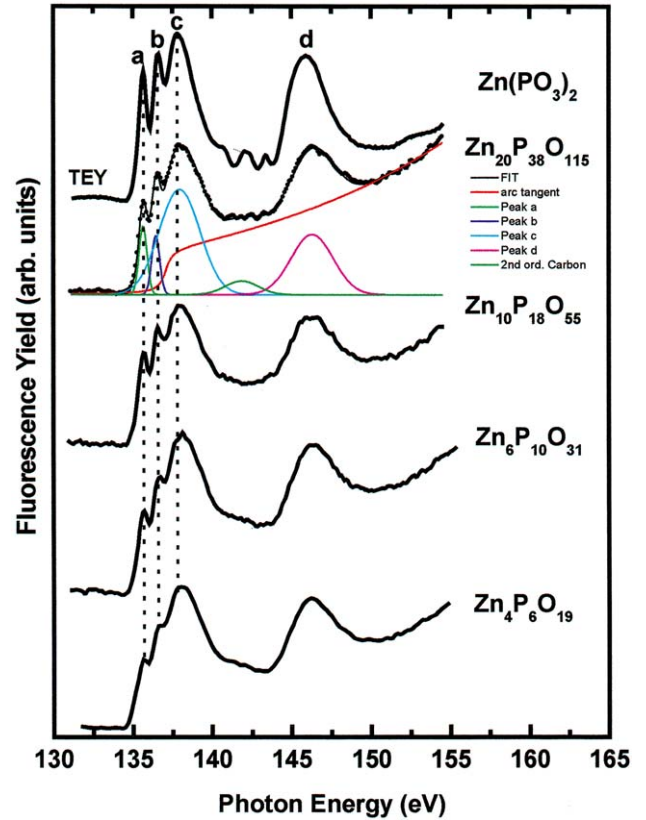
Figure 1. Phosphorus L-edge XANES spectra of synthesized zinc polyphosphate glasses with varying number of phosphorus in the chain length are shown. Also shown is an example of the peak fitting, used to determine the relative peak heights of peaks a, b, and c. A colored version of this figure can be found in the PDF version of this document.

2p level, as well as the local symmetry of the phosphorus. Peaks a and b are the 2p spin–orbit doublet, separated by 0.8 eV. They are assigned to the transitions of electrons from occupied $2p_{3/2}$ and $2p_{1/2}$ levels to unoccupied antibonding orbitals. Peak *c* is attributed to the transition of the 2p electrons of a p-like t_2^* molecular orbital, and peak d is referred to as a d-like shape resonance peak [49]. If the phosphorus is coordinated to three or more electronegative atoms such as oxygen, the shape resonance peak d is shifted to approximately 146 eV. This position is characteristic of all phosphates regardless of their structure, whether crystalline or glassy [50]. On initial comparison, it can be observed that the ratio of relative height of peaks a to c or peaks b to c increases with increasing polyphosphate chain length. To elucidate this trend better, the spectra were fitted by using the BGauss multiline fitting program version 2.3 [51]. The fit for the $Zn_{20}P_{38}O_{115}$ glass is shown. An arc tangent background was positioned at the absorption edge for phosphorus. Peaks a, b, c and d were fitted using Gaussian peaks. Peak a and b were fixed to be equal in width and to have a splitting of 0.8 eV. A Gaussian peak at ~142.5 eV was used to improve the fit and positioned for second-order carbon
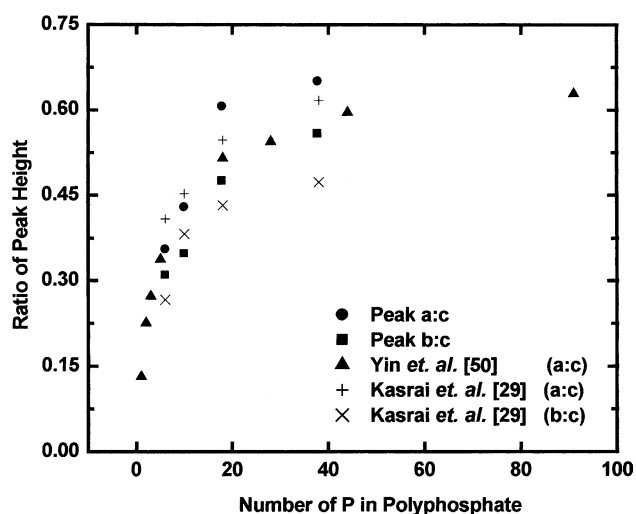
Figure 2. The ratio of the peak height of a:c and b:c are shown as a function of the number of phosphorus in the polyphosphate chain. A trend can be observed in which the ratio of peak heights increases with the increasing number of P in the chain length. Other data reported previously is also plotted.

Figure 3. Phosphorus L-edge XANES spectra of unreacted ZDDP, a zinc metaphosphate ($Zn(PO_3)_2$), zinc polyphosphate ($Zn_{20}P_{38}O_{115}$) model compounds, and the tribofilms on 52100 steel are shown. A difference between the relative peak intensities of peaks a and b to peak c can be observed (see text for discussion).

contamination of the beamline optics. The resulting fit values were used to investigate the relative peak height ratio to the number of P-atoms in the polyphosphate chains. Figure 2 shows the ratio of the relative peak heights plotted versus the number of P in the polyphosphate chain. Results from previous studies are shown [29,50]. The ratio of relative peak heights a:c and b:c both increase with increasing chain length. These trends are in close agreement with those found previously [29,50] (see figure 2). It is important to note that this trend also appears to be independent of the nature of the cation in the phosphate glasses. The results obtained by Yin *et al.* [50] (in figure 2) are for sodium polyphosphate glasses.

The total electron yield (TEY) spectrum for the metaphosphate glass shown in figure 1 has a rather large ratio of relative peak height of peaks a:c ($\sim$0.76); this ratio is practically off scale in figure 2, and may be an indication of the network contained in the polyphosphate structure. It is well known that the metaphosphate glasses contain a three-dimensional structures and the other polyphosphate glasses studied here are two-dimensional [49,52]. We therefore believe that a plateau exists at a peak ratio in a:c and b:c at $\sim$0.6 for even the longest 2-D chains, and that a ratio greater than this may be an indication that the polyphosphate glass contains some three-dimensionality to its structure. A similar result was found for zinc [29] and sodium [50] metaphosphate glasses.

3.2. Film structure

As mentioned above, by use of the different analysis depths of FY and TEY XANES, analysis of ZDDP

antiwear films on steel has shown that the films have a layered structure [13], indicating that ZDDP breaks down to create a polyphosphate film that contains short-chain polyphosphates in the bulk and near substrate regions, and long-chain polyphosphates at the surface. Figure 3, spectrum A, shows the P L-edge spectra for unreacted ZDDP, along with model compounds of a zinc metaphosphate [B] and a zinc polyphosphate [C]. Model compounds are used in XANES spectroscopy to identify the P species present in the antiwear film and help to identify the structure and oxidation state of the phosphorus species. Spectra D and E are the TEY and FY spectra, respectively of an antiwear film. It can be inferred from the presence of peaks a, b, and c in the spectra, that the ZDDP antiwear film has a zinc polyphosphate structure. These peaks are shifted to higher energy compared with peaks 1, 2, and 3 characteristic of unreacted ZDDP. There is no evidence to suggest that iron phosphate is found in our films which would be indicated by a broad pre-edge peak at $\sim$133 eV [53]. Furthermore our K-edge spectra (not shown) did not show a pre-edge peak indicative of iron phosphate [23,53]. An important observation can be made when comparing

spectrum D to E. It can be observed that the ratio of relative peak heights of a:c ($\sim$0.64) in spectrum D is greater than that for the ratio of relative peak heights, of a:c (0.46), in spectrum E. In agreement with previous findings, this indicates that the surface layer of the antiwear film is composed of long-chain polyphosphates and the bulk region is composed of shorter-chain polyphosphates. It is important to point out at this time that the spectra obtained using the Grasshopper beamline are from a large spot size (4 mm $\times$ 1 mm) and represent a global average over the heterogeneous antiwear film surface. The spectra are thus a combination of long-, short-chain polyphosphates and unreacted ZDDP thus providing a mixed signal and poorer resolution of peaks a, b, and c than in the spectra of model compounds in B and C.

Spectrum F was obtained using the X-PEEM, and in the TEY spectrum, probes only the top 5 nm of the surface at the P L-edge. This spectrum has been extracted from the three-dimensional data array (stack) created over the P L-edge region and is an average of several pixels. It can be observed that the spectrum shows the expected polyphosphate peaks a, b and c with an a:c ratio of $\sim$0.60. Furthermore this is in agreement with the TEY spectrum obtained from the global spectrum obtained from the large spot size of the Grasshopper beamline, which indicates that the surface region is composed of long-chain polyphosphates. The high resolution of X-PEEM gives spatially resolved spectra that can be obtained from even one pixel ($\sim$200 nm) and thus result in highly resolved spectra because the data are obtained from a small and therefore laterally more homogenous region. Spectrum F was obtained by averaging several neighbouring pixels, but still shows the high resolution of peaks a, b, and c.

There exist several possible mechanisms for the formation of ZDDP antiwear films from surface adsorption [54,55], thermal degradation [31–33], oxidation by hydroperoxide [56,57], hydrolysis [58], chemical reaction with FeO [59], or a combination of the above [60,61]. Willermet *et al.* [62] have provided the most detailed review of many of the mechanisms on which there *has become* a general agreement. We have previously developed a five step pathway for the decomposition of of ZDDP and formation of a polyphosphate film on steel [63]. In step (i) ZDDP adsorbs to the metallic surface. In step (ii) ZDDP is converted to a linkage isomer in solution, which also (iii) adsorbs onto the metal surface along with the ZDDP. In step (iv) thermal-oxidation of adsorbed linkage isomer and ZDDP occurs by either O_2 or ROOH to form long-chain polyphosphates. In step (v) with continued rubbing, in the presence of water from the base oil, hydrolysis of polyphosphates occurs, creating short-chain polyphosphates. Depending on the conditions of the system the authors also propose that if step (iii) occurs

rapidly, such as in the absence of ZDDP oil-soluble decomposition products, then colloidal, short-chain polyphosphate material can form and be deposited on the surface.

3.3. Chemical mapping

Fiducial marks allowed for relocation of the same area with each technique. AFM topography images were used to identify regions of interest. In figure 4A, a characteristic, large antiwear pad can be observed (Region 1). These are seen as lighter areas which are raised from the surface > 200 nm and are elongated in the rubbing direction. The antiwear film is composed of regions of large antiwear pads (some exceeding the size shown here) and smaller pads. The fiducial grid then allows for the exact region to be relocated with the X-PEEM.

In figure 4B a secondary electron X-PEEM image shows the complexity of the surface. Due to topography,
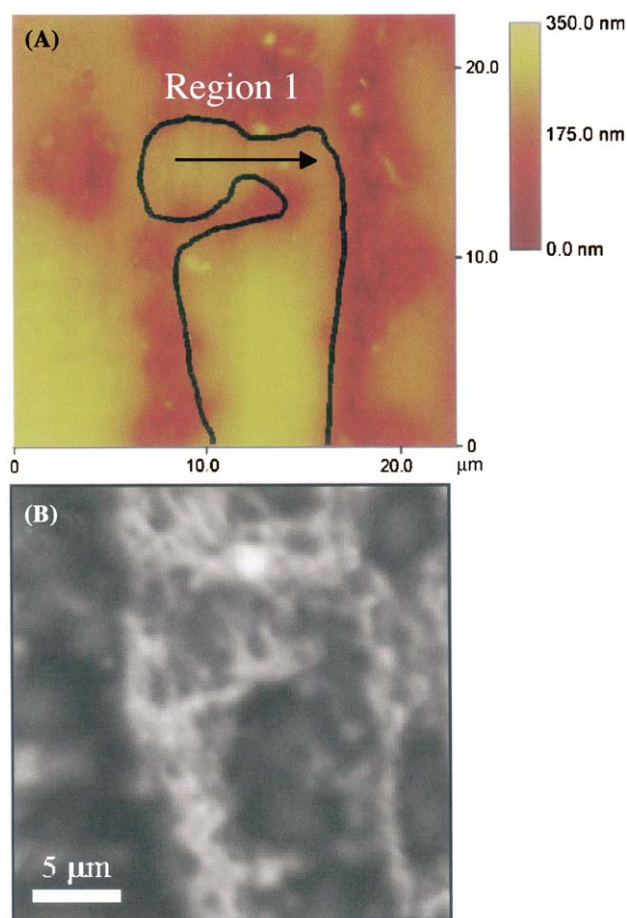
Figure 4. An AFM topography image showing the antiwear pad selected for study is shown in (A) and labeled Region 1. An arrow shows the path along which *f–d* curves were taken. Height and scale bars are provided. Figure (B) shows the corresponding X-PEEM image (secondary electron image) of the same pad. A colored version of this figure can be found in the PDF version of this document.

differential charging resulting from the variable thickness of the insulating pads, shadowing, and chemical variations, the surface does not clearly mimic that observed with AFM imaging. The large antiwear pads, which are composed of polyphosphates, are thick and non-conducting; charging and suppression of secondary electron emission results and these regions of the image appear darker. The large pad (Region 1), of interest, at the center of the image appears as a dark patchy area in the X-PEEM image. Area that have a thinner film, or are flatter, have a larger secondary electron signal and appear brighter in the X-PEEM image due to less charging and/or scattering respectively.

Maps of the long-chain and shorter-chain polyphosphates were obtained by analyzing the image sequence from the P L-edge stack. Analysis using the entire array (all of the images) allows the full P L-edge region to be used in deriving semi-quantitative spatial distributions (maps) of the components. A pixel-by-pixel linear regression procedure, using the singular value decomposition (SVD) technique [64], was used to derive the component maps shown here. The results give semi-quantitative picture of the polyphosphate species at the surface region. The fine spacing of the images (0.1 eV) improves the quality of the linear regression curve fitting of the XANES spectra. XANES model spectra were extracted from the P L-edge stack (internal standard method) which allows for the most accurate mapping when regions of pure material cannot be identified in an area [64]. The software [26,65] also allows for selection of single pixel, or regions of several pixels in size to extract XANES spectra. The spectrum, obtained from regions composed of several pixels, is an average of the signal over all of the pixels selected. Thus, regions were selected that had topographic areas of interest. Such regions included large and small antiwear pads, areas between the antiwear pads, scratch marks, as well as particular dark or bright spots in the X-PEEM image. Differences between the backgrounds obtained from the X-PEEM image and from the model polyphosphate glasses made it difficult to quantitatively determine the polyphosphate chain length in the antiwear film; however a semi-quantitative estimation of the polyphosphate chain length could be determined. The spectra obtained from the chosen regions (composed of several pixels) were compared, and the polyphosphate chain length was determined using the relative peak heights of peaks a:c. Once two spectra, exhibiting significantly different polyphosphate chain lengths (ratio a:c differing by ∼0.2 with good signal to noise ratio), were obtained, these two spectra were then used as internal references with which the component maps were created.

The internal model, long- and shorter-chain spectra are shown in figure 5. These spectra are compared to
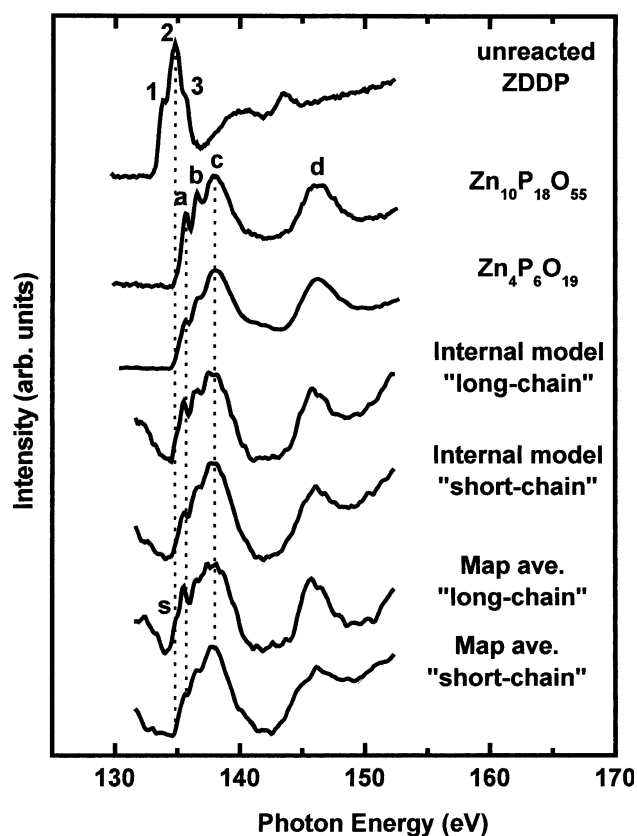
Figure 5. The P L-edge spectra for long-($Zn_{10}P_{18}O_{35}$) and short-($Zn_4P_6O_{19}$) zinc polyphosphate glasses are shown along along with unreacted ZDDP. These spectra are compared to those obtained from the ZDDP antiwear film. The internal long- and short-chain polyphosphate spectra were extracted from the spectromicroscopy stack and used to perform the chemical-species mapping. The map average spectra were obtained after the species distribution maps were performed. A small shoulder, s, indicates that some unreacted ZDDP is located in the same regions as the long-chain polyphosphates (see text for detailed discussion).

unreacted ZDDP, and the synthesized long-($Zn_{10}P_{18}O_{35}$) and short-($Zn_4P_6O_{19}$) chain polyphosphates. The characteristic peaks a, b, c, and resonance peak d can be observed. It is also quite clear that the antiwear film spectra are significantly different than the spectrum of unreacted ZDDP. Component maps were then generated for the long- and shorter-chain polyphosphate distribution in the antiwear film. By use of a signal mask, that was generated for each of the components, corresponding spectra for each component were extracted from multiple pixels and averaged.

These map-average spectra are also shown in figure 5. It can be seen that the map-average spectra quite closely resemble the internal model long- and shorter-chain polyphosphates. A small shoulder, labeled s, which was consistently detected on the map-average long-chain polyphosphate spectra, indicates that a small amount of unreacted ZDDP may also coexist in the areas of long-chain polyphosphate. Since the long-chain polyphosphates are found preferentially
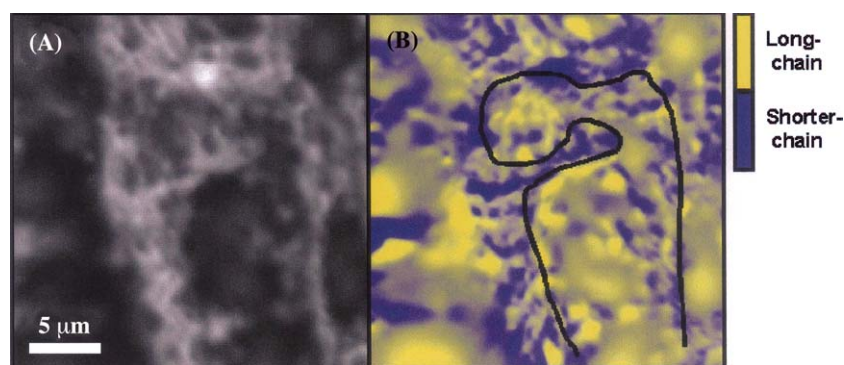
Figure 6. (A) The same X-PEEM image shown in figure 4(B) for Region 1. (B) The distribution map of the long- and shorter-chain polyphosphates in this region of the ZDDP antiwear film. Long-chain polyphosphates are located on the large antiwear pads and shorter-chain polyphosphates are located between the pads. A colored version of this figure can be found in the PDF version of this document.

at the surface, the unreacted ZDDP might be trapped at the surface, and into the surface of the film, at the termination of the rubbing experiment. Presumably if it were simply "smeared" over the surface, it would have been removed by the washing procedure used before the X-PEEM analyses. This may have a small effect on the intensity of peak a, slightly increasing the a:c ratio, but has no effect on the intensity of peak b. We have performed XANES analysis before and after the washing procedure and have not observed any changes in the intensities of peaks a, b, c or, s. This is an indication that the film is very stable which has been observed previously under extending rubbing times in base oil only [66]. Suominen Fuller *et al.* [66] found that a there was little to no change in the thickness of a 30 min. ZDDP tribofilm which was transferred to a base oil alone bath and rubbed for up to 24 h. With this in mind, the evidence is very strong that there are "long-chain" polyphosphates in these areas. We postulate that the long-chain polyphosphate is inter-grown with the shorter-chain (bulk) of the film through P–O–P bonds and metal cations.

The component maps were then digitally combined to produce a polyphosphate distribution map (see figure 6B). In (figure 6A) the secondary electron X-PEEM image showing the large antiwear pad (center) is spatially resolved in terms of polyphosphate chain length and outlined with a black trace, in figure 6B. Yellow in the image indicates long-chain polyphosphates location and blue indicates shorter-chain polyphosphates. Mixtures of both long- and shorter-chain polyphosphates appear as a brown-gray hue in the image. It can be seen that the dark areas of the secondary electron image (representative of extensive and thick antiwear pads) are primarily yellow in the polyphosphate distribution image, indicative of long-chain polyphosphates. In the low topography areas (between the pads) shorter-chain polyphosphates and some intermixing with longer-chain polyphosphates are found. This is the first time that spatially resolved chemical information about ZDDP antiwear films has been determined. We suggest that the

higher pressures and temperatures, experienced during rubbing, are sufficient for the decomposition of ZDDP, and that the highest pressures which are experienced at the surface of the large pads (load-bearing surface) is responsible the creation of the longest chain lengths and possibly for cross-linking of the chains. This result was suggested in earlier work, which found heterogeneity in the elastic response across a large antiwear pad in which the center of the pad was stiffer than the edges [20].

3.4. Nanoindentation

The fiducial marks then allowed for the same region to be located using the imaging nanoindenter. Since X-PEEM (which is XANES analysis on the sub-micron scale) is a non-destructive technique the antiwear film is not disturbed or chemically changed by the soft X-rays. Low-load (50 μN) indentations were performed along the large antiwear pad, in the direction indicated on figure 4A (Region 1). The 16 force–displacement (f–d) curves gave an indentation modulus (E_s^*) of 80.5 $\pm$ 4.5 GPa. At a load of 50 μN, penetration into the film was $\sim$15 nm with a contact depth (h_c) calculated to be 12 nm, which is on the order of 10% of the film thickness.

The thickness of the antiwear pad was determined from the AFM topography image to be $\sim$115 nm. Multiple cross-sectional profiles were taken across the pad, in which the film thickness was conservatively estimated from the top of the pad to halfway down the valley. If it is assumed that the bottom of the valley contains some shorter-chain polyphosphates this method still underestimates the thickness of the pad. Using equations (4)–(7) the modulus of the film (E_f), separated from the steel substrate, was determined to be 67.4 GPa. Figure 7 shows a representative f–d curve for Region 1 identified above, also included is a f–d curve for representative of the regions identified by arrows in figure 8B (Region 2 to be discussed below). The f–d curve taken on polished steel at the same load
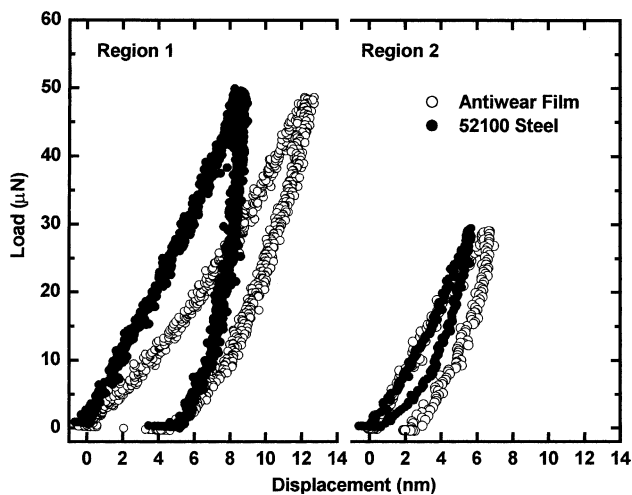
Figure 7. A representative *f–d* curve taken along the path shown in figure 4(A) for Region 1 is shown. This force curve is compared to a similar one taken on polished 52100 steel. Differences in the initial slope of the unloading curve and hysteresis can be observed. Likewise, a *f–d* curve representative of that found in Region 2 (see figure 8) is compared to a curve taken in 52100 steel. Note the elastic response is very similar in the later case.

is also compared to the *f–d* curve of the film in Region 1. It can be observed that the initial slope of the withdrawal curve is shallower than that on steel indicating a softer material. The elastic modulus of 52100 steel is ~220 GPa. The value obtained for the antiwear film is similar to that found by others [19,20,23] for indentations taken to similar maximum loads and on the same apparent-size antiwear pads. The distribution map indicates that Region 1 contains mostly long-chain polyphosphates with some intermixing with shorter-chain. The *f–d* curves taken along this region had penetration depths that only slightly exceeding the analysis depth of the X-PEEM. Therefore we suggest that the mechanical response measured here is characteristic of the elastic response of long-chain polyphosphates. This represents the first chemo-mechanical characterization of ZDDP antiwear pads! We further suggest that it is these properties, of the large antiwear pads, which are beneficial for preventing wear of asperities by maintaining a spacer layer between the rubbing surfaces. It has been observed previously that shorter-chain polyphosphate films, such as those formed in the presence of detergent, have poor antiwear performance [67].

Region 2 was chosen because it is composed of smaller antiwear pads located between large pads (see figure 8A and B). Figure 8B is the topographic AFM image showing the small pad area outlined in black. Component mapping was performed using the same internal model spectra since the two regions were located on the same spectromicroscopy stack. Again, it can be observed that the long-chain polyphosphate is located at the regions where the large antiwear pads are found, and the shorter-chain polyphosphates are located between the large pads. Regions were selected

to further investigate the trend found with the distribution map and thus spectra were extracted from the areas containing many pixels. Figure 8C shows these selected regions, cross-hatched and numbered. The resultant spectra, averaged over all the pixels in each region, are shown in figure 8D. Semi-quantitative, relative peak height ratios of peaks a:c are also listed.

When these extracted spectra were compared to the internal model spectra, shown in figure 5, there is again evidence for the presence of unreacted ZDDP. In the spectra obtained from areas 2, 4 and 5 the smaller shoulder (labeled s) at the low energy side of peak a indicates that some unreacted ZDDP is found in these areas. This is consistent with the idea that areas between the pads had not been subjected to the load and shearing forces required to fully decompose ZDDP. This may also suggest a reason as to why ZDDP is such an effective antiwear agent since ZDDP can be found in crevices which act as reservoirs during the rubbing process. Similar results to this were found on rough steel surfaces that were rubbed under similar tribological conditions to those used here [2]. The authors suggested that unreacted ZDDP was trapped in the valleys between asperities. Early X-PEEM work performed on rough steel with ZDDP also found that unreacted ZDDP was found in the wear scar intermixed with the polyphosphate film [68]. A further conclusion can be drawn from these spectra. The large a:c relative peak height ratios (>0.6) may indicate that not only are long-chain polyphosphates found on the large antiwear pads, but that they may in fact actually be comprised partially of 3-D polyphosphates (see the zinc metaphosphate spectrum in figure 1 and discussion above).

Nanoindentation experiments were performed along the arrows shown in figure 8B. Force curves were taken to maximum loads of 30 μN. This load was chosen since the film was determined (from topography imaging; see Method described above) to be thinner (~85 nm) than Region 1, and thus lower-load *f–d* curves are required to sample the film's mechanical properties without any influence from the substrate. A great deal of scatter was found in the E_s^* values calculated from these curves. We believe that this scatter results from the fact that the film is too thin to permit accurate measurements of the mechanical properties to be made with the current nanoindenter, and that future work using an interfacial force microscope [19,69–71] is required. The IFM can perform indentations at much lower loads and penetration depths and also yields mechanical property values by analyzing the approach curve, thus permitting more accurate measurements to be made on the thin antiwear film located between the large antiwear pads. Previous work using an IFM found that the areas located between the large antiwear pads contained smaller pads (as seen in figure 8B) but also a softer, plastically
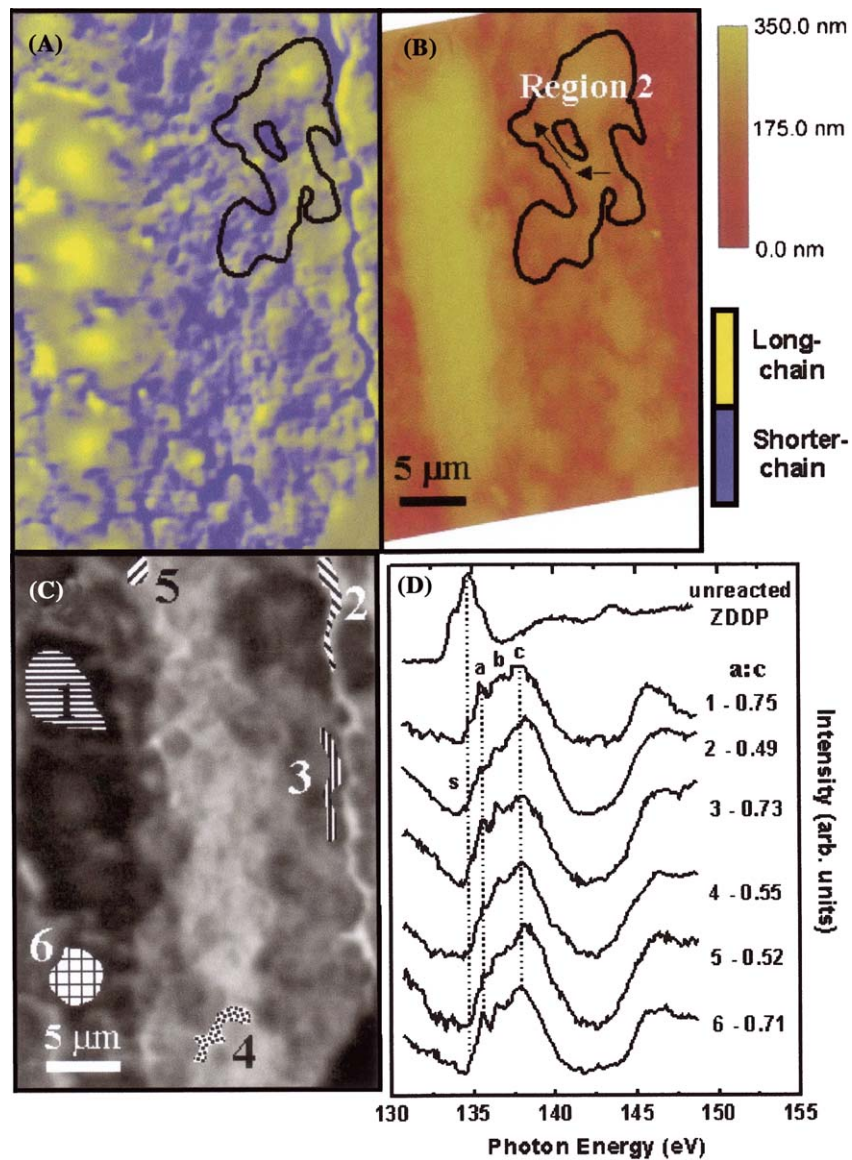
Figure 8. In (A) the polyphosphate distribution map can be observed. This is compared to the AFM topography image (B). The selected Region 2 is outlined. Arrows indicated the paths along which *f–d* curves were taken. (C) The X-PEEM image and areas that were selected to extract spectra from. The corresponding spectra to the cross-hatched areas are shown in (D). The ratios of the relative peak heights of a:c are also shown. A colored version of this figure can be found in the PDF version of this document.

deformable material that had an indentation modulus ~30 GPa [19,21]. The authors suggested that this was a mixture of wear debris and unreacted, or partially decomposed ZDDP.

An example of the *f–d* curves measured for Region 2 is shown in figure 7. Comparison to a *f–d* curve taken into 52100 steel, at the same load, shows that the response of the film, at this load, is very similar to that of steel, even though the approach curve shows a softer material is present, further indicating that we may actually be sensing the steel substrate as well. At these loads, the penetration into the film was < 8 nm and difficulties in fitting the initial portion of the withdrawal curve using the Oliver and Pharr method may have been related to the fact that the tip area function was

not accurately known at such low penetration depths. Further work fitting the initial portion of the approach curve using Hertzian contact mechanics using IFM, and from calibrations of the geometry of the Berkovich tip, may help to extract more accurate values.

4. Conclusion

We have reported the first chemo-mechanical mapping of ZDDP antiwear films. The results found here will help to elucidate the origins of the effectiveness of ZDDP antiwear films. XANES analysis of model zinc polyphosphate glasses showed that the relative peak heights of peaks a:c in the P L-edge spectra increase with increasing number of P in the polyphosphate

chain. These data were used to semi-quantitatively determine the chain length of the polyphosphate glasses making up the antiwear pads. AFM topography imaging was used to locate areas of interest and to determine the approximate film thickness. Fiducial marks placed on the surface of the wear scar allowed for relocation of the same film features with multiple techniques. The films were then examined with X-PEEM which provided non-destructive chemical analysis via the P L-edge at ~200 nm lateral resolution per pixel. Polyphosphate distribution maps were created to examine the lateral location of polyphosphates in the antiwear film. It was found that the higher (antiwear) pads had a larger concentration of long-chain polyphosphates than the lower (valley) regions which had shorter-chain polyphosphates. Further investigation found that the valley regions found between the large pads had not only shorter-chain polyphosphates, but also showed evidence of some unreacted ZDDP. This suggests that these regions act like reservoirs for ZDDP and that when the large pads shear away, unreacted ZDDP is there to replenish and reform new antiwear pads.

An imaging nanoindenter allowed for the mechanical properties of these same features to be examined on the same spatial scale. Indentations performed along a large antiwear pad gave an indentation modulus (E_s^*) of 80.5 ± 4.5 GPa which gives an $E_f = 67.4$ GPa if we assume that the steel substrate may be influencing the mechanical response of the film. This value is in agreement with that found by others [19–21,23,24]. This allowed for the first correlation between the elastic response of the film and the polyphosphate chain length to be made.

These results show how X-ray emission microscopy has allowed the sub-micron resolution of the chemical speciation in a ZDDP antiwear film to be correlated with nanoscale mechanical testing of the same features. These results shed new light on the effectiveness of ZDDP antiwear film formation and wear protection mechanisms, and may provide insight into how new ashless additives need to work in order to perform as effectively as ZDDP. Further work investigating polyphosphate chain length and the mechanical response of the thinner regions of the films needs to be performed to help understand the film properties. We have initiated a program of theoretical studies to model the mechanical properties of the various glasses.

Acknowledgments

References

[1] Z. Yin, M. Kasrai, G.M. Bancroft, K.F. Laycock and K.H. Tan, Trib. Int. 26 (1993) 383.

[2] Z. Yin, M. Kasrai, M. Fuller, G.M. Bancroft, K. Fyfe and K.H. Tan, Wear 202 (1997) 172.

[3] M. Fuller, Z. Yin, M. Kasrai, G.M. Bancroft, E.S. Yamaguchi, P.R. Ryason, P.A. Willermet and K.H. Tan, Trib. Int. 30 (1997) 305.

[4] J.M. Martin, Trib. Lett. 6 (1999) 1.

[5] J.M. Martin, T.Le Mogne, C. Grossiord and T. Palermo, Trib. Lett. 2 (1996) 313.

[6] S. Jahanmir, J. Trib. 109 (1987) 577.

[7] C. Grossiord, J.M. Martin, T. Le Monge and T. Palermo, Trib. Lett. 6 (1999) 171.

[8] Q.J. Xue and M.W. Bai, Wear 195 (1996) 66.

[9] J.S. Sheasby, M.C. Jennings and K.D. Cassells, Wear 231 (1999) 256.

[10] J.M. Martin, J.L. Mansot, I. Berbezier and H. Dexpert, Wear 93 (1984) 117.

[11] S.H. Choa, K.C. Ludema, G.E. Potter, B.M. DeKoven, T.A. Morgan and K.K. Kar, Wear 177 (1994) 33.

[12] J.C. Bell and K.M. Delargy, in: *The 6th International Congress on Tribology*, "Eurotrib '93" (1993).

[13] G.M. Bancroft, M. Kasrai, M. Fuller, Z. Yin, K. Fyfe and K.H. Tan, Trib. Lett. 3 (1997) 47.

[14] E.S. Ferrari, K.J. Roberts and D. Adams, Wear 236 (1999) 246.

[15] E.S. Ferrari, K.J. Roberts and D. Adams, Wear 253 (2002) 759.

[16] J.S. Sheasby, T.A. Caughlin and W.A. Mackwood, Wear 196 (1996) 100.

[17] J.S. Sheasby, T.A. Caughlin and W.A. Mackwood, Wear 201 (1996) 209.

[18] Y.Y. Yang, Y.S. Jin and T. Yan, Wear 210 (1997) 136.

[19] O.L. Warren, J.F. Graham, P.R. Norton, J.E. Houston and T.A. Michalske, Trib. Lett. 4 (1998) 189.

[20] J.F. Graham, C. McCague and P.R. Norton, Trib. Lett. 6 (1999) 149.

[21] S. Bec, A. Tonck, J.M. Georges, R.C. Coy, J.C. Bell and G.W. Roper, Proc. Roy. Soc. Lond. A 455 (1999) 4181.

[22] A. Tonck, S. Bec, J.M. Georges, R.C. Coy, J.C. Bell and G.W. Roper, in: *Tribology Series: Lubrication at the Frontier*, Vol. 36, eds. D. Dowson (Elsevier Science B.V., Amsterdam, 1999) 39.

[23] M.A. Nicholls, T. Do, P.R. Norton, G.M. Bancroft, M. Kasrai, T.W. Capehart, Y.-T. Cheng and T. Perry, Trib. Lett. 15 (2003) 241.

[24] S. Bec and A. Tonck, in: *Tribology Series: Lubricants and Lubrication*, Vol. 30, eds. Dowson, C. Taylor, T. Childs and G. Dalmaz (Elsevier, Amsterdam, 1996) 173.

[25] C. Morin, H. Ikeura-Sekiguchi, T. Tyliszczak, R. Cornelius, J.L. Brash, A.P. Hitchcock, A. Scholl, F. Nolting, G. Appel, D.A. Winesett, K. Kaznacheyev and H. Ade, J. Elect. Spectro. Relat. Phenom. 121 (2001) 203.

[26] L.M. Croll, J.F. Britten, C. Mortin, A.P. Hitchcock and H.D.H. Stoever, J. Synchro. Rad. 10 (2003) 265.

[27] C. Jacobsen, S. Wirick, G. Flynn and C. Zimba, J. Microsc. 197 (2000) 173.

[28] X. Zhang, R. Balhorn, J. Mazrimas and J. Kirz, J. Struct. Bio. 116 (1996) 335.

[29] M. Kasrai, M. Fuller, M. Scaini, Z. Yin, R.W. Brunner, G.M. Bancroft, M.E. Fleet, K. Fyfe and K.H. Tan, in: *Lubricants and Lubrication: Lubrication at the Frontier,* Vol. 30, eds. D. Dowson, et al. (Elsevier Science B.V., Amsterdam, 1995) 659.

[30] M. Kasrai, W.N. Lennard, R.W. Brunner G.M. Bancroft, J.A. Bardwell and K.H. Tan, Appl. Surf. Sci. 99 (1996) 303.

[31] B.H. Frazer, B. Gilbert, B.R. Sonderegger and G. De Sthasio, Surf. Sci. 537 (2003) 161.

[32] W.C. Oliver and G.M. Pharr, J. Mater. Res. 7 (1992) 1564.

[33] A.V. Kulkarni and B. Bhushan, Mat. Lett. 29 (1996) 221.

[34] J. Malzbender and G. de With, Surf. Coatings Technol. 135 (2000) 60.

[35] J. Mencik, D. Munz, E. Quandt, E.R. Weppelmann and M.V. Swain, J. Mater. Res. 12 (1997) 2475.

[36] T. Chudoba, N. Schawarzer and F. Richter, Surf. Coatings Technol. 127 (2000) 9.

[37] G.M. Pharr and W.C. Oliver, MRS Bull. 17 (1992) 28.

[38] A.M. Korsunsky, M.R. McGurk, S.J. Bull and T.F. Page, Surf. Coatings Technol. 99 (1998) 171.

[39] T. Chudoba, N. Schawarzer, F. Richter and U. Beck, Thin Solid Films 377–378 (2000) 366.

[40] J. Malzbender and G. de With, Surf. Coatings Technol. 127 (2000) 266.

[41] S. Bec, A. Tonck, J.-M. Georges and J.-L Loubet, Phil. Mag. A 74 (1996) 1061.

[42] A. Rar, H. Song and G.M. Pharr, in: *Materials Research Society Symposium Proceedings* (2002), 431.

[43] H. Gao, C.-H. Chiu and J. Lee, Int. J. Solids Struct. 29 (1992) 2471.

[44] J.W. Wiench, M. Pruski, B. Tischendorf, J.U. Otaigbe and B.C. Sales, J. Non-Cryst. Solids 263&264 (2000) 101.

[45] B.C. Sales, J.U. Otaigbe, D.M. Beall, L.A. Boatner and J.O. Ramey, J. Non-Cryst. Solids 226 (1998) 287.

[46] B. Tischendorf, J.U. Otaigbe, J.W. Wiench, M. Pruski and B.C. Sales, J. Non-Cryst. Solids 282 (2001) 147.

[47] A. Feltz, *Structure and Chemical Bonding in Glasses and Amorphous Solids*, Vol. l (VCH, New York, 1993).

[48] E.C. Onyiriuka, J. Non-Cryst. Solids 163 (1993) 268.

[49] D.G.J. Sutherland, M.Kasrai, G.M. Bancroft, Z.F. Liu and K.H. Tan, Phys. Rev. B 48 (1993) 14989.

[50] Z. Yin, M. Kasrai, G.M. Bancroft, K.H. Tan and X. Feng, Phys. Rev. B 51 (1995) 742.

[51] T. Tyliszczak, *BGAUSS – Multiline Fitting Program,* Unpublished Version 2.3 (1994).

[52] A. Feltz, in: *Amorphous Inorganic Materials and Glasses*, Vol. 1, (VCH, 2100) 72.

[53] M.N. Najman, M. Karsai, G.M. Bancroft and A. Miller, Trib. Lett. 13 (2002) 209.

[54] B. Dacre and C.H. Bovington, ASLE Trans. 26 (1983) 333.

[55] C.H. Bovington and B. Dacre, ASLE Trans. 27 (1984) 252.

[56] J.J. Habeeb and W.H. Stover, ASLE Trans. 30 (1987) 419.

[57] J.L. Paddy, N.J.C. Lee, D.N. Waters and W. Trott, Trib. Trans. 33 (1990) 15.

[58] H. Spedding and R.C. Watkins, Trib. Int. February (1982) 9.

[59] W.A. Glaeser, D. Baer and M. Engelhardt, Wear 162–164 (1993) 132.

[60] I. Sieber, K. Meyer, H. Kloss and A. Schopke, Wear 85 (1983) 43.

[61] P.A. Willermet, R.O. Carter III and E.N. Boulos, Trib. Int. 25 (1992) 371.

[62] P.A. Willermet, D.P. Dailey, R.O. Carter III and P.J. Schmitz and W. Zhu, Trib. Int. 28 (1995) 177.

[63] M.L. Suominen Fuller, M. Kasrai, G.M. Bancroft, K. Fyfe and K.H. Tan, Trib. Int. 31 (1998) 627.

[64] I.N. Koprinarov, A.P. Hitchcock, C.T. McCrory and R.F. Childs, J. Phys. Chem. B. 106 (2002) 5358.

[65] A.P. Hitchcock, P. Hitchcock, C. Jacobsen, C. Zimba, B. Loo, E. Rotenberg, J. Denlinger and R. Kneedler, *aXis2000 – program available from http://unicorn.mcmaster.ca/aXis2000.html* (1997)

[66] M.L. Suominen Fuller, L.R. Fernandez, G.R. Massoumi, W.N. Lennard and M. Kasrai, Trib. Lett. 8 (2000) 187.

[67] Y. Wan, M. L. Suominen Fuller, M. Kasrai, G.M. Bancroft, K. Fyfe, J.R. Torkelson, Y.F. Hu and K.H. Tan, in: *Boundary and Mixed Lubrication: Science and Applications*, Vol. 40, eds. D. Dowson (Elsevier Science B.V., 2002) 155.

[68] G.W. Canning, M.L. Fuller, G.M. Bancroft, M. Kasrai, J.N. Cutler, G. De Stasio and B. Gilbert, Trib. Lett. 6 (1999) 159.

[69] P. Tangyunyong, R.C. Thomas, J.E. Houston, T.A. Michalske and R.M. Crooks, Phys. Rev. Lett. 71 (1993) 3319.

[70] J.E. Houston and T.A. Michalske, Nature 356 (1992) 266.

[71] R.C. Thomas, J.E. Houston, T.A. Michalske and R.M. Crooks, Science 259 (1993) 1883.